Cognition-Driven Formulation of Space Mapping for Equal-Ripple Optimization of Microwave Filters

Chao Zhang, *Student Member, IEEE*, Feng Feng, *Student Member, IEEE*, Venu-Madhav-Reddy Gongal-Reddy, Qi Jun Zhang, *Fellow, IEEE*, and John W. Bandler, *Life Fellow, IEEE*

***Abstract*—Space mapping is a recognized method for speeding up electromagnetic (EM) optimization. Existing space-mapping approaches belong to the class of surrogate-based optimization methods. This paper proposes a cognition-driven formulation of space mapping that does not require explicit surrogates. The proposed method is applied to EM-based filter optimization. The new technique utilizes two sets of intermediate feature space parameters, including feature frequency parameters and ripple height parameters. The design variables are mapped to the feature frequency parameters, which are further mapped to the ripple height parameters. By formulating the cognition-driven optimization directly in the feature space, our method increases optimization efficiency and the ability to avoid being trapped in local minima. The technique is suitable for design of filters with equal-ripple responses. It is illustrated by two microwave filter examples.**

***Index Terms*—Cognition-driven design, computer-aided design (CAD), electromagnetic (EM) optimization, microwave filters, modeling, space mapping (SM).**

I. Introduction

SPACE MAPPING (SM) is a recognized engineering optimization methodology in the microwave area [1]–[3]. The SM concept combines the computational efficiency of coarse models with the accuracy of fine models [1]. Coarse models are typically empirical functions or equivalent circuits, which are computationally efficient but demonstrate low accuracy. Fine models can be provided by an electromagnetic (EM) simulator, which is accurate but computationally intensive. SM establishes a mathematical link between the coarse and fine models and directs the bulk of the CPU-intensive computations to the coarse models, while preserving the accuracy from the fine models [2]. Recent progress has focused on several areas, such as a recent review points towards a cognition interpretation of SM [4], portable SM for efficient modeling [5], three-level output SM [6], tuning SM [7], shape-preserving response prediction [8], parallel SM [9] and zero-pole SM [10]. A software implementation of space mapping such as the SMF framework with applications such as antenna design have also been described in the literature [11].

In practical cases, equivalent circuit coarse models are not always available [12]. Some effort has been focused on this situation. In [13], to build a coarse model for waveguide filters, a small number of accessible modes in the method of moments are considered to obtain a faster simulation at the expense of solution accuracy. In the work of [12], [14]–[16], coarse and fine mesh EM simulations are used to enable space mapping EM optimization. Sensitivity information from EM simulations has been used to increase the effectiveness of space mapping [15], [17], [18]. The convergence speed in this case is affected by the difference between fine and coarse mesh EM simulations, and the continuity of the coarse mesh EM response w.r.t design variables.

This paper is a significant advance over the work of [15] in an effort to address the challenge of SM when explicit equivalent circuit coarse models are not available. We exploit the concept of feature parameters to assist the SM, as opposed to use of coarse-mesh EM in [15]. Several recent works have investigated possible feature parameters in model responses. In [19], using the differences between return loss and transmission loss at maxima in the passband and minima in the stopband as the objective function, the coefficients of the characteristic polynomial for a filter are optimized to reach equiripple passband and stopband responses. Theories for the synthesis of multiple coupled resonator filters go back many years [20], [21], and zeros and poles of filter transfer functions are used as feature parameters for optimization in [10] and [22]. In [23] and [24], feature parameters of filter responses are used for SIW filter tuning and statistical analysis of microwave structures.

This paper aims to explore the use of intermediate feature space parameters in SM. We propose a cognition-driven formulation of space mapping for equal-ripple optimization of microwave filters. It is suitable for EM-based design of Chebyshev- and elliptic-type responses. The proposed SM can proceed with neither explicit coarse models nor explicit

Manuscript received December 06, 2014; revised April 16, 2015; accepted April 24, 2015. Date of publication June 02, 2015; date of current version July 01, 2015. This work was supported in part by the Natural Sciences and Engineering Research Council of Canada under Grant RGPIN 122049-09, Grant RGPIN7239-11, and Grant STPGP447367-13, Tianjin University, and Bandler Corporation.

C. Zhang and V.-M.-R. Gongal-Reddy are with the Department of Electronics, Carleton University, Ottawa, ON K1S5B6, Canada (e-mail: chaozhang@doe.carleton.ca; vmgongal@doe.carleton.ca).

F. Feng is with the Department of Electronics, Carleton University, Ottawa, ON K1S5B6, Canada, and also with the School of Electronic Information Engineering, Tianjin University, Tianjin, China (e-mail: fengfeng@doe.carleton.ca).

Q. J. Zhang was with the School of Electronic Information Engineering, Tianjin University, Tianjin, China, on leave from the Department of Electronics, Carleton University, Ottawa, ON K1S5B6, Canada (e-mail: qjz@doe.carleton.ca).

J. W. Bandler is with the Simulation Optimization Systems Research Laboratory and Department of Electrical and Computer Engineering, McMaster University, Hamilton, ON L8S 4K1, Canada, and also with Bandler Corporation, Dundas, ON L9H 5E7, Canada (e-mail: bandler@mcmaster.ca).

Color versions of one or more of the figures in this paper are available online at http://ieeexplore.ieee.org.

Digital Object Identifier 10.1109/TMTT.2015.2431675

surrogate models. In our method, the intermediate feature space parameters, including the feature frequency parameters and ripple height parameters, are used to set up two new kinds of space mapping. The design variables are mapped to feature frequency parameters, which are further mapped to the ripple height parameters, thus the concept of SM in our optimization. By formulating the cognition-driven optimization directly in the feature space, our method can increase optimization efficiency and ability to avoid being trapped in local minima. This technique is illustrated by two microwave bandpass filter examples.

We think of our technique as "cognitive" [4] in the sense that a meaningful coarse or surrogate model is implied by the engineer's intuition and experience.

This paper is organized as follows. In Section II, the design optimization problem is outlined, and the challenges of EM optimization are described. In Section III, our proposed cognition-driven formulation of SM for microwave filter optimization is introduced, and details of the new algorithm are provided. In Section IV, we demonstrate the EM optimization of two microwave bandpass filter examples, confirming the efficiency of our proposed approach to cognition-driven optimization.

II. Original Optimization Problem

Let $R(\boldsymbol{x}, \omega)$ denote the response corresponding to a vector of design variables $\boldsymbol{x}$ and frequency ω. The original optimization problem is formulated as follows:

$$\boldsymbol{x}^* = \arg\min_{\boldsymbol{x}} U\left(R(\boldsymbol{x}, \omega)\right) \tag{1}$$

where U is a suitable objective function, typically minimax objective function [25], which represents the error function of $R(\boldsymbol{x}, \omega)$ with respect to the design specifications, and $\boldsymbol{x}^*$ is the optimal design to be found.

The convergence of optimization is efficient when the objective functions are relatively smooth and/or the initial values are of good quality. However, when the objective functions contain traps of local minima and the initial values are not within the neighborhood of a good solution, gradient-based optimization may easily be trapped into local solutions. An example is the filter design shown in Fig. 1(a), (c), and (e). As shown in the figures, because the reflection zeros of the four-pole filters are not all within the specification range, the optimization process will force only three poles to contribute to the filter passband response, while the remaining one pole is excluded from helping the passband response. Suitable optimization techniques, such as nongradient-based methods, may help alleviate some of the above-mentioned problems, usually at the cost of longer CPU time. In this paper, we explore an efficient approach to solve the problem using feature parameters and formulations inspired by human design intuition.

III. Proposed Space Mapping Technique for Microwave Optimization

A. Feature Space Parameters

Our cognition-driven approach is motivated by the intuitive (cognitive) design process of the experienced filter designer.

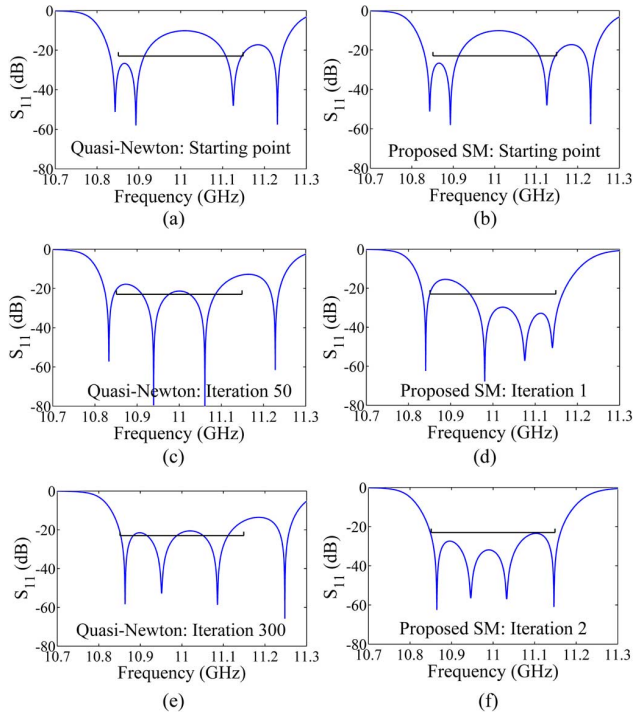

Fig. 1. Optimization of the four-pole waveguide filter: (a), (c), (e) Responses during quasi-Newton optimization iterations, where only three poles are forced to contribute passband response: (a) initial, (c) iteration 50, (e) and iteration 300. (b), (d), and (f) Proposed cognition-driven space mapping iterations. (d) Proposed method adjusts the frequency locations of reflection zeros to the passband in the first stage. (f) Then the frequency locations of reflection zeros are adjusted according to the ripple height parameters.

The designer would firstly adjust the frequency locations of reflection zeros relative to the passband, rather than trying to push the S-parameter values in the initial design stage. In subsequent design stages, the designer would adjust the ripple height using the fact that making two frequency locations of reflection zeros closer (further apart) will reduce (increase) the height of the passband ripple in the frequency response curve. This process is illustrated in Fig. 1(b), (d), and (f). By adopting such a concept, we reformulate the design optimization by introducing new feature parameters for the design, i.e., we define a new feature parameter space, called the feature frequency space as follows.

For an equal-ripple bandpass filter, the filter response curve (e.g., S_{11} versus frequency) has several minima which are referred to as feature frequencies, and several maxima which are referred to as ripples. The feature frequencies correspond to the reflection zeros at which the filter has maximum transmission. We propose to use feature frequencies as feature space parameters for space mapping. For example, Fig. 2(a) shows a four-pole waveguide filter, and Fig. 2(b) shows S_{11} in decibels of this filter, where the feature frequencies $\boldsymbol{f} = [f_1\ f_2\ f_3\ f_4]^T$ are important features of the S_{11} response curve and are used by our technique as intermediate feature space for a new formulation of space mapping. We perform space mapping between physical/geometrical design variables $\boldsymbol{x}$ (i.e., the original optimization variables) and the feature frequency parameters $\boldsymbol{f}$.

The maximum values of S_{11} in decibels between these feature frequency points are also important features of the S_{11} response curve and are represented by a new set of feature parameters

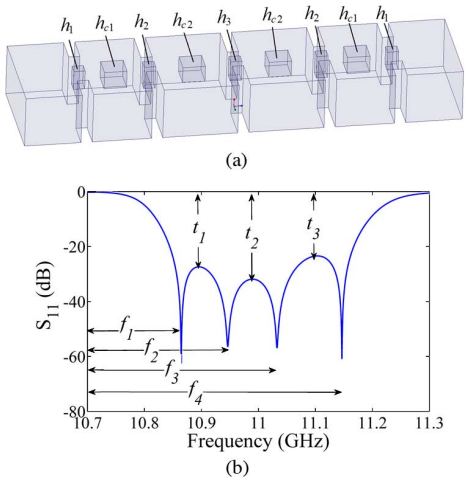

Fig. 2. Four-pole waveguide filter. (a) Simulation structure. (b) Proposed feature parameters $\boldsymbol{t}$ and $\boldsymbol{f}$ in the filter response.

called ripple height parameters $\boldsymbol{t} = [t_1\ t_2\ t_3]^T$ similar to that used in [23] and [24].

In our proposed formulation of space mapping, we obtain the feature frequency parameters $\boldsymbol{f} = [f_1\ f_2 \cdots f_M]^T$ and the ripple parameters $\boldsymbol{t} = [t_1\ t_2 \cdots t_{M-1}]^T$ from the results of an EM simulation, where M represents the number of poles of the filter.

At the beginning of our proposed method, we generate multiple sample points with star distribution around the current solution point $\boldsymbol{x}^{(k)}$ in the kth iteration of space mapping. We perturb $\boldsymbol{x}^{(k)}$ twice along each dimension, once towards the positive direction, and once towards the negative direction. In this way, we find $2N$ points of response, where N is the number of design variables. Let $\boldsymbol{x}_1, \boldsymbol{x}_2, \ldots, \boldsymbol{x}_{2N+1}$ represent the $2N+1$ points of the star distribution with $\boldsymbol{x}_1$ as the center, i.e., $\boldsymbol{x}_1 = \boldsymbol{x}^{(k)}$, and the remaining $2N$ points in the neighborhood of the center. When the optimization process moves to the next iteration, the center of the star distribution moves from $\boldsymbol{x}^{(k)}$ to $\boldsymbol{x}^{(k+1)}$. We perform EM simulations at all the $2N+1$ data points to obtain the responses $R(\boldsymbol{x}_i, \omega)$ at $\boldsymbol{x}_i$, using $2N+1$ processors in parallel [9], and subsequently obtain $\boldsymbol{f}_i$ and $\boldsymbol{t}_i$, for $i = 1, 2, \ldots, 2N+1$. In this way, the basic data available in the kth iteration includes the feature frequency parameters $\boldsymbol{f}^{(k)}$ and the ripple height parameters $\boldsymbol{t}^{(k)}$, which equal $\boldsymbol{f}_1$ and $\boldsymbol{t}_1$, respectively. Because our algorithm uses parallel computation to perform the $2N+1$ EM simulations simultaneously, the total computation time for the $2N+1$ EM simulations is similar to (or only incrementally more than) that of a single EM simulation.

B. Mapping from $\boldsymbol{f}$ Space to the $\boldsymbol{x}$ Space

With this basic data, we can build the mapping $\boldsymbol{F}$ from the design variables $\boldsymbol{x} = [x_1\ x_2\ \cdots\ x_N]^T$ to the feature frequency parameters $\boldsymbol{f}$ as follows:

$$\boldsymbol{f} = \boldsymbol{F}(\boldsymbol{x}) \tag{2a}$$

$$\boldsymbol{A} = \frac{\partial \boldsymbol{F}^T(\boldsymbol{x})}{\partial \boldsymbol{x}}. \tag{2b}$$

$\boldsymbol{A} \in M_{M\times N}$ is the Jacobian matrix of $\boldsymbol{F}$. We evaluate the $\boldsymbol{A}$ matrix using the EM solutions over the $2N+1$ star distribution points as

$$[\boldsymbol{A}]_{m,n} = \frac{[F_m(\boldsymbol{x} + \Delta\boldsymbol{x}_n) - F_m(\boldsymbol{x} - \Delta x_n)]}{2\Delta\boldsymbol{x}_n}, \quad m = 1, 2, \cdots, M;\ n = 1, 2, \cdots, N \tag{3}$$

where F_m is the mth element of $\boldsymbol{F}$, and Δx_n is the perturbation of x_n in the star distribution. $\Delta\boldsymbol{x}_n$ is defined as a vector containing zero everywhere except the nth element, which is Δx_n, i.e.,

$$\Delta\boldsymbol{x}_n = \begin{bmatrix} 0 & \cdots & \overset{(n)}{\Delta x_n} & \cdots & 0 \end{bmatrix}^T, \qquad n = 1, 2, \cdots, N. \tag{4}$$

We incorporate the trust region mechanism [26] into our formulation of optimization. When this mapping $\boldsymbol{F}$ is built, we can solve for the step $\boldsymbol{s}^{(k)}$ in the kth iteration by

$$\boldsymbol{s}^{(k)} = \arg \min_{\|\boldsymbol{s}\| \le \delta^{(k)}} \left\| \boldsymbol{f}_d^{(k)} - \boldsymbol{f}^{(k)} - \boldsymbol{A}^{(k)}\boldsymbol{s} \right\| \tag{5}$$

where $\delta^{(k)}$ is the trust radius, $\boldsymbol{f}_d^{(k)}$ represents the desired frequency vector, and $\boldsymbol{A}^{(k)}$ is the Jacobian matrix of $\boldsymbol{F}$ in the kth iteration.

C. Stage 1: Adjustment of Locations of Feature Frequencies

In the first stage, the passband specified for the filter is divided into $(M-1)$ equal parts. The desired feature frequency parameters $\boldsymbol{f}_d^1$ in the first stage are designated as

$$\boldsymbol{f}_d^1 = [\, f_L \quad f_L + \tfrac{f_H - f_L}{M-1} \quad \cdots \quad f_L + \tfrac{f_H - f_L}{M-1}(M-2) \quad f_H \,]^T \tag{6}$$

where f_L and f_H mean the lower and higher frequency edge of the filter passband, respectively. Both f_L and f_H are constants determined *a priori* according to the desired filter passband. Now we can calculate $\boldsymbol{s}^{(k)}$ by solving (5) using $\boldsymbol{f}_d^{(k)} = \boldsymbol{f}_d^1$ for the first stage.

Once $\boldsymbol{s}^{(k)}$ is determined, we generate $2N+1$ sample points with star distribution in parallel around the new center $(\boldsymbol{x}^{(k)} + \boldsymbol{s}^{(k)})$and perform these $2N+1$ EM simulations in parallel. The feature frequency parameters $\boldsymbol{f}_s^{(k)}$ and the ripple height parameters $\boldsymbol{t}_s^{(k)}$ are determined at $(\boldsymbol{x}^{(k)} + \boldsymbol{s}^{(k)})$.

Then, we calculate the adjustment index r for the trust radius as part of the trust region procedure. If the dimensions of feature space parameters change, r is set to be -1. Otherwise, r can be obtained by

$$r = \frac{U_1\left(\boldsymbol{f}^{(k)}\right) - U_1\left(\boldsymbol{f}_s^{(k)}\right)}{U_1\left(\boldsymbol{f}^{(k)}\right) - U_1\left(\boldsymbol{f}^{(k)} + \boldsymbol{A}^{(k)}\boldsymbol{s}^{(k)}\right)} \tag{7}$$

where U_1 is the objective function for the first stage defined as

$$U_1(\boldsymbol{f}) = \left\| \boldsymbol{f}_d^1 - \boldsymbol{f} \right\|. \tag{8}$$

The stopping criterion for the first stage is shown as follows:

$$\left| f_1^{(k)} - f_L \right| + \left| f_M^{(k)} - f_H \right| \le \varepsilon_1 \tag{9}$$

where ε_1 is a user-defined threshold for the first stage. By doing this, all of the feature frequency points will move to the passband, and $\boldsymbol{f}$ will have approximately equal distance between each two adjacent feature frequency points. Therefore, the first stage helps to avoid being trapped in a local minimum.

D. Stage 2: Mapping from $\boldsymbol{t}$ Space to $\boldsymbol{f}$ Space and Adjustment of Ripple Height

In the second stage, we perform the second kind of mapping, i.e., from the feature frequency parameters to the ripple height parameters as follows:

$$\boldsymbol{B}^{(k)}\left(\boldsymbol{f}_d^{(k)}-\boldsymbol{f}^{(k)}\right)+\boldsymbol{c}^{(k)}=\boldsymbol{t}_a-\boldsymbol{t}^{(k)} \tag{10}$$

where $\boldsymbol{t}_a \in M_{(M-1)\times 1}$ represents the desired ripple height parameters, and $\boldsymbol{B}^{(k)} \in M_{(M-1)\times(M)}$ and $\boldsymbol{c}^{(k)} \in M_{(M-1)\times 1}$ are mapping coefficients between the $\boldsymbol{f}$ and $\boldsymbol{t}$ spaces. To find the optimal filter solution, the ripples should be equal, which means every element of $\boldsymbol{t}^{(k+1)}$ should be the same. Let $\overline{t}$ be defined as the average value of $\boldsymbol{t}^{(k)}$, i.e.,

$$\overline{t}=\frac{1}{M-1}\sum_{i=1}^{M-1}t_i \tag{11}$$

To make every element of $\boldsymbol{t}_a$ equal, we set

$$\boldsymbol{t}_a=\left[\,\overline{t}\quad\overline{t}\quad\cdots\quad\overline{t}\,\right]^T. \tag{12}$$

By doing this, we translate optimization problem (1) into the $\boldsymbol{t}$ space with a new criterion, which is that the variance $Var(\boldsymbol{t}^{(k)})$ of $\boldsymbol{t}^{(k)}$ is minimized to be smaller than a user-defined threshold ε_2

$$Var\left(\boldsymbol{t}^{(k)}\right)=\frac{1}{M-1}\sum_{t=1}^{M-1}(t_i-\overline{t})^2\le\varepsilon_2 \tag{13}$$

When this new criterion is reached, the optimization process stops. If not, we determine the mapping between the $\boldsymbol{t}$ space and the $\boldsymbol{f}$ space. To do this, we firstly determine the matrix $\boldsymbol{B}^{(k)}$ and vector $\boldsymbol{c}^{(k)}$ by the following training process:

$$\left(\boldsymbol{B}^{(k)},\boldsymbol{c}^{(k)}\right)=\arg\min_{(\boldsymbol{B},c)}\varepsilon_t(\boldsymbol{B},c) \tag{14}$$

where the training error function is defined as

$$\varepsilon_t(\boldsymbol{B},\boldsymbol{c})=\sum_{i=2}^{2N+1}\left\|\boldsymbol{B}(\boldsymbol{f}_i-\boldsymbol{f}_1)+\boldsymbol{c}-(\boldsymbol{t}_i-\boldsymbol{t}_1)\right\|. \tag{15}$$

After $\boldsymbol{B}^{(k)}$ and $\boldsymbol{c}^{(k)}$ are found from (14) and (15), the mapping between the $\boldsymbol{t}$ and $\boldsymbol{f}$ spaces is determined. We will use the mapped $\boldsymbol{f}$ to deduce the desired value of the $\boldsymbol{f}$ vector, for the feature parameters in the $\boldsymbol{f}$ space. We introduce a new vector $\Delta\boldsymbol{f}=\left[\,\Delta f_1\quad\Delta f_2\quad\cdots\quad\Delta f_M\,\right]^T$, which satisfies

$$\boldsymbol{f}_d^{(k)}=\boldsymbol{f}^{(k)}+\Delta\boldsymbol{f} \tag{16}$$

where $\boldsymbol{f}_d^{(k)}$ represents the desired frequency vector and $\boldsymbol{f}^{(k)}$ represents the current actual frequency parameters. In order to find $\boldsymbol{f}_d^{(k)}$ in the second stage, we need to solve for $\Delta\boldsymbol{f}$. After the first stage, we assume that (9) is satisfied. Therefore, any changes to Δf_1 and Δf_M will influence the passband. We need to refine the values of Δf_1 and Δf_M according to $R(\boldsymbol{x}^{(k)},\omega)$. First, we find two frequency points f_l and f_h in the EM responses which can satisfy

$$f_l=\min\left\{\omega_j|R\left(\boldsymbol{x}^{(k)},\omega_j\right)\le\overline{t}<R\left(\boldsymbol{x}^{(k)},\omega_{j-1}\right)\right\} \tag{17a}$$

$$f_h=\max\left\{\omega_j|R\left(\boldsymbol{x}^{(k)},\omega_j\right)\le\overline{t}<R\left(\boldsymbol{x}^{(k)},\omega_{j+1}\right)\right\} \tag{17b}$$

where $j=1,2,\ldots,N_f$, and N_f is the number of frequency points per EM simulation. These two frequencies f_l and f_h, approximately representing the lower and upper frequencies of the current frequency band, are compared with the desired lower and upper frequencies f_L and f_H. Then, Δf_1 and Δf_M are obtained by solving

$$\Delta f_1=f_L-f_l \tag{18a}$$

$$\Delta f_M=f_H-f_h. \tag{18b}$$

Equations (17) and (18) try to refine the passband location. Then we regard Δf_1 and Δf_M as constant value and obtain $\Delta\boldsymbol{f}$ by solving

$$\begin{aligned}\Delta\boldsymbol{f}=\arg\min_{\Delta f_2,\cdots,\Delta f_{M-1}}\Big\|&\boldsymbol{t}_a-\boldsymbol{t}^{(k)}\\&-\boldsymbol{B}^{(k)}\left[\Delta f_1\ \Delta f_2\ \cdots\ \Delta f_{M-1}\ \Delta f_M\right]^T\\&-\boldsymbol{c}^{(k)}\Big\|.\end{aligned} \tag{19}$$

Using (16), $\boldsymbol{f}_d^{(k)}$ can be obtained from $\Delta\boldsymbol{f}$.

Next, we perform SM from the $\boldsymbol{f}$ space to the $\boldsymbol{x}$ space by solving (5).

Once $\boldsymbol{s}^{(k)}$ is determined, we perform $2N+1$ EM simulations using the star distribution in parallel around the new center $(\boldsymbol{x}^{(k)}+\boldsymbol{s}^{(k)})$, and subsequently we can get the feature frequency parameters $\boldsymbol{f}_s^{(k)}$ and the ripple height parameters $\boldsymbol{t}_s^{(k)}$ at $(\boldsymbol{x}^{(k)}+\boldsymbol{s}^{(k)})$.

We calculate the adjustment index r for the trust radius. If the dimensions of feature space parameters change, r is set to be -1. Otherwise, r can be obtained by

$$r=\frac{U_2\left(\boldsymbol{t}^{(k)}\right)-U_2\left(\boldsymbol{t}_s^{(k)}\right)}{U_2\left(\boldsymbol{t}^{(k)}\right)-U_2\left(\boldsymbol{t}^{(k)}+\boldsymbol{B}^{(k)}\boldsymbol{A}^{(k)}\boldsymbol{s}^{(k)}+\boldsymbol{c}^{(k)}\right)} \tag{20}$$

where U_2 is defined as

$$U_2(\boldsymbol{t})=Var(\boldsymbol{t}). \tag{21}$$

Notice that the computation for trust region parameters in Stage 2 [described by (20) and (21)] are different from that in Stage 1 [described by (7) and (8)].

E. Update of Trust Region

After we get $\boldsymbol{s}^{(k)}$ for both stages, we should update the radius of the trust region using the following equation [26], [27]:

$$\delta^{(k+1)}=\begin{cases}0.618\left\|\boldsymbol{s}^{(k)}\right\|, & \text{if } r<0.1\\ \min\left\{1.214\delta^{(k)},\Delta^*\right\}, & \text{if } r>0.8\\ \left\|\boldsymbol{s}^{(k)}\right\|, & \text{otherwise}\end{cases} \tag{22}$$

where Δ^* is the maximum value of the trust radius and decide whether or not to accept this step $\boldsymbol{s}^{(k)}$.

If the dimension of $\boldsymbol{f}_s^{(k)}$ remains the same as $\boldsymbol{f}^{(k)}$, and the following condition:

$$U_1\left(\boldsymbol{f}_s^{(k)}\right) \le U_1\left(\boldsymbol{f}^{(k)}\right) \tag{23}$$

is satisfied in the first stage or the condition

$$Var\left(\boldsymbol{t}_s^{(k)}\right) \le Var\left(\boldsymbol{t}^{(k)}\right) \tag{24}$$

is satisfied in the second stage, we accept the step $\boldsymbol{s}^{(k)}$ and update the design variables as

$$\boldsymbol{x}^{(k+1)} = \boldsymbol{x}^{(k)} + \boldsymbol{s}^{(k)}. \tag{25}$$

At the same time, we set $\boldsymbol{f}^{(k+1)} = \boldsymbol{f}_s^{(k)}$, and $\boldsymbol{t}^{(k+1)} = \boldsymbol{t}_s^{(k)}$.

In this way, both the original design variables and the trust radius are updated, thereby completing one iteration of the proposed space mapping.

Otherwise (i.e., if the dimensions of feature space parameters change, or neither (23) nor (24) is satisfied), $\boldsymbol{x}^{(k)}$ will be kept unchanged, and a new $\boldsymbol{s}^{(k)}$ is calculated by solving (5) with the updated trust radius $\delta^{(k)} = \delta^{(k+1)}$.

To make our proposed method more robust, we terminate the algorithm if one of the following conditions is satisfied: $\|\boldsymbol{x}^{(k+1)} - \boldsymbol{x}^{(k)}\| < 10^{-2}$ or $\delta^{(k+1)} < 10^{-3}$ [28].

F. Stepwise Algorithm

The flowchart of the proposed space mapping technique is shown in Fig. 3. The proposed algorithm can be summarized as follows.

Step 1) Initialize $\boldsymbol{x}^{(k)}$ and $\delta^{(k)}$ at $k = 0$.

Step 2) Set $\boldsymbol{x}_1$ to be equal to $\boldsymbol{x}^{(k)}$. Create multiple points $\boldsymbol{x}_1, \boldsymbol{x}_2, \ldots, \boldsymbol{x}_{2N+1}$ using a star distribution sampling strategy with the center $\boldsymbol{x}_1$. Evaluate multi-point fine responses $R(\boldsymbol{x}_i, \omega)$ by performing EM simulation using parallel computation for $i = 1, 2, \ldots, 2N+1$.

Step 3) Determine the feature frequency parameters $\boldsymbol{f}^{(k)}$ and the ripple height parameters $\boldsymbol{t}^{(k)}$.

Step 4) If the stopping criterion of the first stage (9) is not satisfied, go to step 5), else go to step 9).

Step 5) Obtain the first mapping matrix $\boldsymbol{A}^{(k)}$ by solving (3)–(4) and get $\boldsymbol{f}_d^1$ by (6).

Step 6) Obtain the prospective step $\boldsymbol{s}^{(k)}$ by solving (5).

Step 7) Perform parallel EM simulations at $2N+1$ star distribution points around the new center $(\boldsymbol{x}^{(k)} + \boldsymbol{s}^{(k)})$. Obtain the feature parameters $\boldsymbol{f}_s^{(k)}$ and $\boldsymbol{t}_s^{(k)}$ at $(\boldsymbol{x}^{(k)} + \boldsymbol{s}^{(k)})$, and find r using (7)–(8). Update trust radius $\delta^{(k+1)}$ by solving (22) according to the value of r.

Step 8) If the dimension of $\boldsymbol{f}_s^{(k)}$ remains the same as $\boldsymbol{f}^{(k)}$, and $U_1(\boldsymbol{f}_s^{(k)}) \le U_1(\boldsymbol{f}^{(k)})$, then we update the design variable $\boldsymbol{x}^{(k+1)} = \boldsymbol{x}^{(k)} + \boldsymbol{s}^{(k)}$, set $\boldsymbol{f}^{(k+1)} = \boldsymbol{f}_s^{(k)}$, and set $\boldsymbol{t}^{(k+1)} = \boldsymbol{t}_s^{(k)}$. Update iteration counter $k = k+1$, and go to step 4). Otherwise, keep $\boldsymbol{x}^{(k)}$ unchanged, set $\delta^{(k)} = \delta^{(k+1)}$, and go to step 6).

Step 9) If the stopping criterion of the second stage (13) is satisfied, STOP, otherwise, go to step 10).

Step 10) Obtain $\boldsymbol{A}^{(k)}$ by solving (3)–(4) and get the second set of mapping matrices $\boldsymbol{B}^{(k)}, \boldsymbol{c}^{(k)}$ by solving (14)–(15), then find $\boldsymbol{f}_d^{(k)}$ by solving (10)–(12) and (16)–(19).

Step 11) Obtain the prospective step $\boldsymbol{s}^{(k)}$ by solving (5).

Step 12) Perform parallel EM simulations at $2N+1$ star distribution points around the new center $(\boldsymbol{x}^{(k)} + \boldsymbol{s}^{(k)})$. Get the feature parameters $\boldsymbol{f}_s^{(k)}$ and $\boldsymbol{t}_s^{(k)}$ at $(\boldsymbol{x}^{(k)} + \boldsymbol{s}^{(k)})$, and find r using (20)–(21). Update trust radius $\delta^{(k+1)}$ by solving (22) according to the value of r.

Step 13) If the dimension of $\boldsymbol{f}_s^{(k)}$ remains the same as $\boldsymbol{f}^{(k)}$, and $Var(\boldsymbol{t}_s^{(k)}) \le Var(\boldsymbol{t}^{(k)})$, then we update the design variables $\boldsymbol{x}^{(k+1)} = \boldsymbol{x}^{(k)} + \boldsymbol{s}^{(k)}$, set $\boldsymbol{f}^{(k+1)} = \boldsymbol{f}_s^{(k)}$, and set $\boldsymbol{t}^{(k+1)} = \boldsymbol{t}_s^{(k)}$. Update iteration counter $k = k+1$, and go to step 9). Otherwise, keep $\boldsymbol{x}^{(k)}$ unchanged, set $\delta^{(k)} = \delta^{(k+1)}$, and go to step 11).

G. Discussion

There are two kinds of challenges for EM optimization of filter design, the first being the challenge of a computationally bad starting point, but one with the correct number of feature frequencies, and the second the ability to correct the number of feature frequencies if the initial point has the wrong number of feature frequencies. In this paper, we focus on the solution to the first challenge. The second challenge, which is equally important and a heavy task, is a possible direction of future research. In our present work, we have used an empirical approach to preprocess the starting point using derivative information of the response shape to guide the correction of the number of the feature frequencies iteratively. Once the correct number of feature frequencies is reached, the proposed trust region method in the two different optimization stages will maintain the number of feature frequencies throughout the proposed optimization process.

IV. Examples

A. Optimization of a Four-Pole Waveguide Filter

The first example under consideration is a four-pole waveguide filter [13]. The tuning elements are penetrating posts of square cross section placed at the center of each cavity and each coupling window, shown in Fig. 2(a). The input and output waveguides, as well as the resonant cavities, are standard WR-75 waveguides ($a = 19.050$ mm, $b = 9.525$ mm). The thickness of all of the coupling windows is set to 2 mm. h_1, h_2, and h_3 are the heights of posts in the coupling windows, and h_{c1}, h_{c2} are the height of the posts in the resonant cavities. The design variables are $\boldsymbol{x} = [\, h_1 \quad h_2 \quad h_3 \quad h_{c1} \quad h_{c2} \,]^T$.

If the EM simulation uses discrete frequency simulation, then sufficiently small frequency steps are needed to detect all feature frequency points. In our work, the EM evaluation is performed by the *ANSYS HFSS* EM simulator using the fast simulation feature. With this simulation feature, we can get the S-parameter response over the entire frequency range of interest without a discrete frequency sweep. Such a fast frequency sweep uses an adaptive Lanczos-Padé sweep (ALPS)-based solver to extrapolate the field solution across the requested frequency range from the center frequency field solution. The desired filter responses have been chosen to be standard four-pole Chebyshev curves of

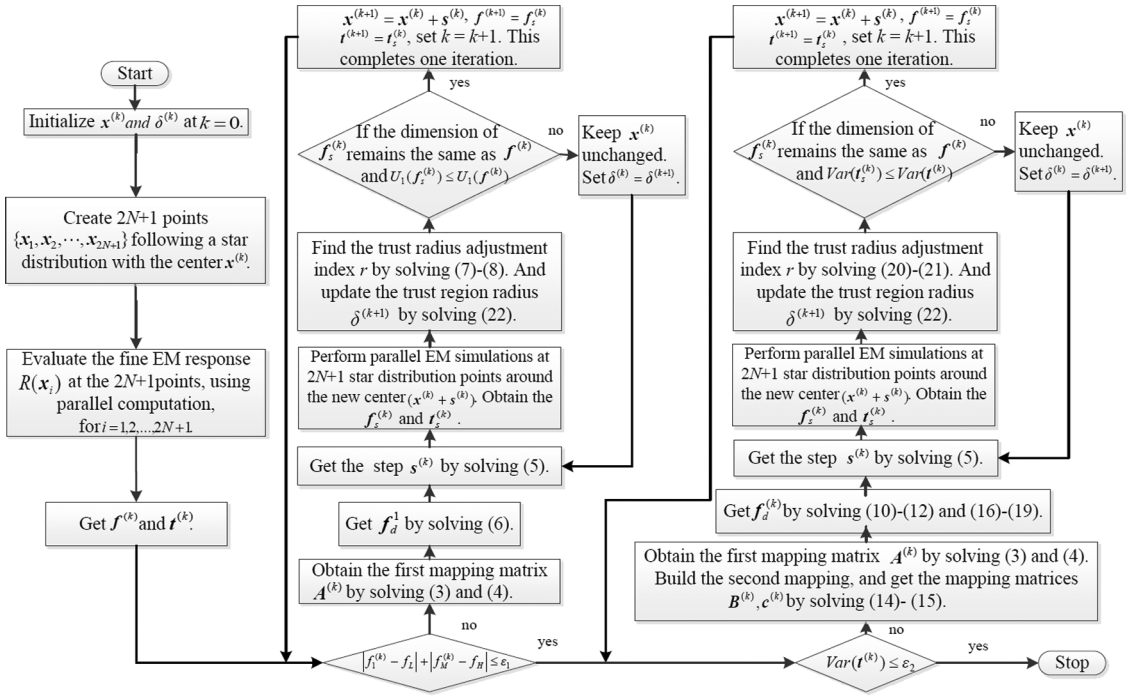

Fig. 3. Flowchart of the proposed cognition-driven space mapping technique.

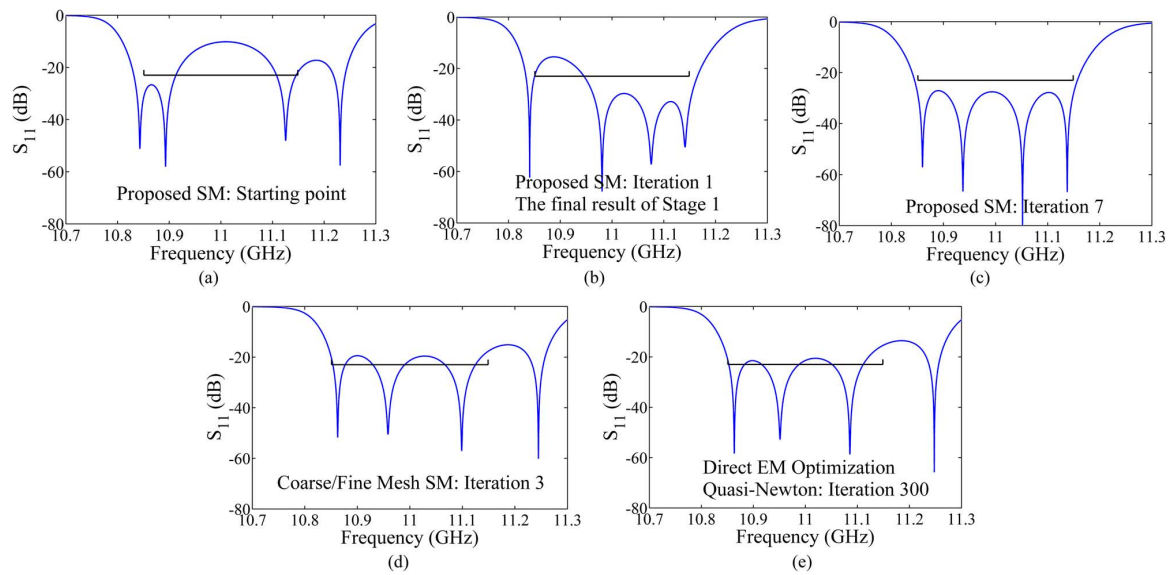

Fig. 4. Comparison of the results for three different optimization methods for the four-pole waveguide filter example. (a) Starting point for all three methods. (b) Using our proposed space mapping method, all of the feature frequencies move to the passband after the first stage. (c) A good equal-ripple response is obtained after seven iterations, and our method can avoid being trapped in a local minimum. (d) Using coarse and fine mesh space mapping, the optimization process falls into a local minimum. (e) Using direct EM optimization, the optimization process falls into a local minimum.

300-MHz bandwidth, 0.02-dB ripple, and centered at 11 GHz. The specification on the magnitude of S_{11} in the passband is -23.4 dB, corresponding to 0.02-dB ripple in S_{21}. The starting point is $\boldsymbol{x}^{(0)} = [3.3\ 4.389\ 3.991\ 3.28\ 2.914]^T$ (all values in millimeters). From the second iteration, the $\boldsymbol{t}$ parameters are found to be $\boldsymbol{t}^{(2)} = [-15.473\ \ -29.709\ \ -32.851]^T$ (all values in decibels).

Using the proposed technique, the optimal solution $\boldsymbol{x}^{(7)} = [3.562\ 4.291\ 3.790\ 3.237\ 2.955]^T$ (all values in millimeters) is obtained after seven iterations, and the final ripple vector $\boldsymbol{t}^{(7)} = [-27.088\ \ -27.512\ \ -27.783]^T$ (all values in decibels). The responses from the initial point, the first and the last iterations are shown in Fig. 4(a)–(c), respectively. Fig. 4(b) shows that all of the feature frequencies move to the passband after the first iteration. Fig. 4(c) shows that our proposed method can avoid being trapped in a local minimum and that a good equal-ripple filter response is obtained after seven iterations. The values of objective function for all of the iterations are shown in Fig. 5. From the figure, we observe that using our proposed space mapping method the filter response can satisfy the design specifications in two iterations and it can even exceed the specifications in subsequent iterations. U_1 in the first stage and

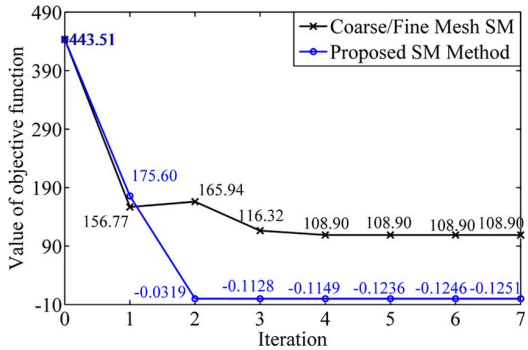

Fig. 5. Objective function values of the four-pole waveguide filter response using: the proposed SM method (o) and coarse and fine mesh space mapping method (x). The objective function in the coarse and fine mesh space mapping optimization cannot be reduced further because it falls into a local minimum. Our proposed method can avoid being trapped in a local minimum and finds a good filter response in seven iterations.

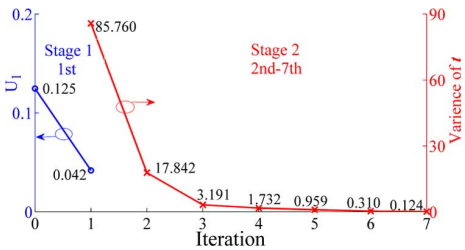

Fig. 6. Feature space objective functions U_1 and U_2 (i.e., $Var(\boldsymbol{t})$) for the four-pole waveguide filter example. The first stage goes in the first iteration, and the second stage runs from the second iteration to the seventh iteration. Both U_1 and $Var(\boldsymbol{t})$ converge fast.

the variances of $\boldsymbol{t}$ in the second stage of our proposed method are shown in Fig. 6. We set the threshold $\varepsilon_2 = 0.2$. Smaller (or larger) values for ε_2 tend to make the ripple heights more (or less) uniform using more (or less) overall computation time. In this example, both U_1 and the variance of $\boldsymbol{t}$ converge fast.

For comparison purposes, we use the baseline coarse and fine mesh space mapping optimization method [14] to optimize this filter. The coarse mesh EM optimizations for the surrogate training and for surrogate optimization are both carried out using High-Frequency Structure Simulator's (HFSS's) internal quasi-Newton optimizer. The value of the objective function for each iteration is shown in Fig. 5, from which we found that the coarse and fine mesh space mapping optimization process falls into a local minimum. The space mapping iterations stopped at this point because the updates by surrogate optimization cannot lead to any improvement in the fine model responses. The comparison of the results for different methods, including direct EM optimization (using HFSS Optimetrics quasi-Newton optimization), coarse and fine mesh space mapping method and our proposed method is shown in Fig. 4 and Table I. In the coarse and fine mesh SM method, the training time and the design optimization time are very long because of coarse mesh EM simulation. In our method, the training process, which means solving mapping matrices $\boldsymbol{A}$, $\boldsymbol{B}$, and $\boldsymbol{c}$, and the design optimization process, which is to solve (5), only do algebraic calculations, so our feature SM method saves much time. Our proposed method uses eleven (i.e., $2N+1$) EM simulations per iteration, which is more

TABLE I
COMPARISONS OF THREE METHODS FOR THE WAVEGUIDE FILTER

Optimization Method	Direct EM Optimization	Coarse/Fine Mesh Space Mapping	Proposed Space Mapping
No. of Iterations	300	4	7
Fine Model Evaluation Time	300× 4min	5× 4min	8× 6min
Training Time	-	3× 1h	7× 1min
Design Optimization Time	-	4× 1h	7× 1min
Total Time	20 h	7 h 20 min	1h 2 min
Final Value of Objective Function	69.14 (being trapped in local minimum)	108.90 (being trapped in local minimum)	-0.1251

than by existing techniques, such as coarse and fine mesh space mapping. Because these eleven simulations are completely independent of each other, our technique is well suited for parallel computation, making the total computation time (6 min) for the 11 EM simulations to be only incrementally more than a single EM simulation (4 min). The total number of optimization iterations is much reduced in our technique because of the increased amount of useful information available from $2N + 1$ EM simulations in each iteration. As observed in Table I, our method can increase the optimization efficiency and find a better result within less time compared to coarse and fine mesh EM SM and direct EM optimization.

As a further experiment about robustness of the proposed optimization for this filter example, we use a much worse starting point $\boldsymbol{x}^{(0)} = [3.020\ \ 4.680\ \ 4.314\ \ 3.480\ \ 3.028]^T$ (all values in mm) to rerun our proposed method. Using the proposed technique, the optimal solution $\boldsymbol{x}^{(8)} = [3.424\ \ 4.116\ \ 3.608\ \ 3.291\ \ 2.977]^T$ (all values in millimeters) is obtained after eight iterations, and the final ripple vector $\boldsymbol{t}^{(8)} = [-24.316\ \ -24.062\ \ -24.793]^T$ (all values in decibels). The responses from the initial point, the last iteration of the first stage and the last iteration of proposed method are shown in Fig. 7(a)–(c), respectively. A preprocessing step was used to create a usable starting point, which is shown in Fig. 7(a), with the correct number of feature frequencies, i.e., four. During the optimization process, if EM simulations occasionally produce the wrong number of (e.g., three) feature frequencies, our trust region mechanism will shrink the step size until the number of feature frequencies returns to 4, at which point the optimization update then takes place. Fig. 7(b) shows that all of the feature frequencies move to the passband after the first stage. Fig. 7(c) shows that our proposed method can avoid being trapped in local minima and that a good equal-ripple filter response is obtained after eight iterations. The values of objective function for all the iterations are shown in Fig. 8. From the figure, we observe that using our proposed space mapping method the filter response can satisfy the design specifications in eight iterations. U_1 in the first stage and the variances of $\boldsymbol{t}$ in the second stage of our proposed method are shown in Fig. 9.

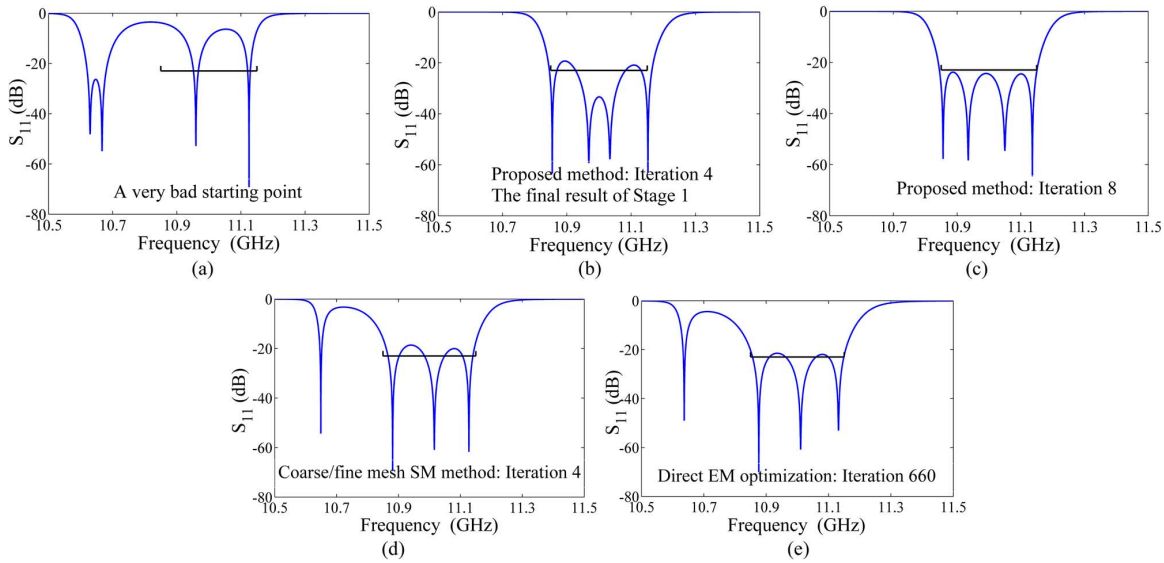

Fig. 7. Comparison of the results for three different optimization methods for the four-pole waveguide filter example with bad starting point. (a) Bad starting point for all three methods. (b) Using our proposed SM method, all of the feature frequencies move to the passband after the first stage. (c) Good equal-ripple response is obtained after eight iterations, and our method can avoid being trapped in a local minimum. (d) Using coarse and fine mesh space mapping, the optimization process falls into a local minimum. (e) Using direct EM optimization, the optimization process falls into a local minimum.

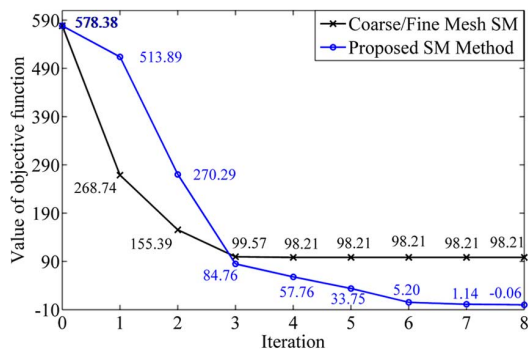

Fig. 8. Objective function values of the four-pole waveguide filter response with bad starting point using: the proposed space mapping method (o) and coarse and fine mesh space mapping method (x). The objective function in the coarse and fine mesh SM optimization cannot be reduced further because it falls into a local minimum. Our proposed method can avoid being trapped in a local minimum and finds a good filter response in eight iterations.

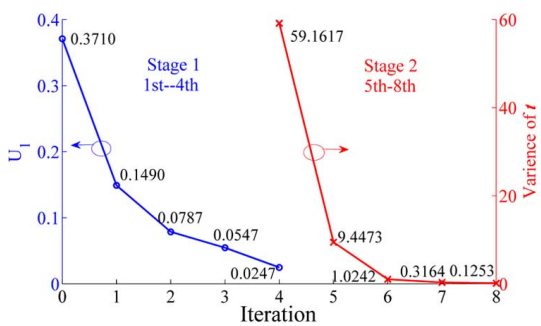

Fig. 9. Feature space objective functions U_1 and U_2(i.e., $Var(\boldsymbol{t})$) for the four-pole waveguide filter example with bad starting point. The first stage goes from the first iteration to the fourth iteration, and the second stage runs from the fifth iteration to the eighth iteration. Both U_1 and $Var(\boldsymbol{t})$ converge fast.

For comparison purposes, we also use the baseline coarse and fine mesh SM optimization method [14] to optimize this filter. The value of objective function for each iteration is shown in Fig. 8, from which we found that the coarse and fine mesh space mapping optimization process falls into a local minimum with filter responses still violating design specifications. We also performed direct EM optimization of this filter example for a further comparison. With the same starting point and same design specifications, the direct EM optimization also falls into a local minimum with filter responses violating design specifications. The comparison of the results for different methods, including direct EM optimization, coarse and fine mesh space mapping method and our

TABLE II
COMPARISONS OF THREE METHODS FOR THE WAVEGUIDE FILTER WITH BAD STARTING POINT

Optimization Method	Direct EM Optimization	Coarse/Fine Mesh Space Mapping	Proposed Space Mapping
No. of Iterations	660	4	8
Fine Model Evaluation Time	660× 4min	5× 4min	(9+6*)× 6min
Training Time	-	3× 1h	8× 1min
Design Optimization Time	-	4× 1h	8× 1min
Total Time	44 h	7 h 20 min	1h 46 min
Final Value of Objective Function	25.42 (being trapped in local minimum)	98.21 (being trapped in local minimum)	-0.06

*The number of EM simulations, which are not accepted during trust region adjustment

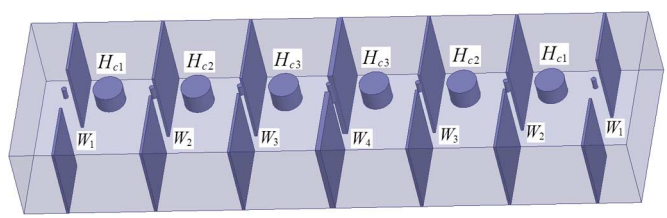

Fig. 10. Structure of the waveguide cavity filter.

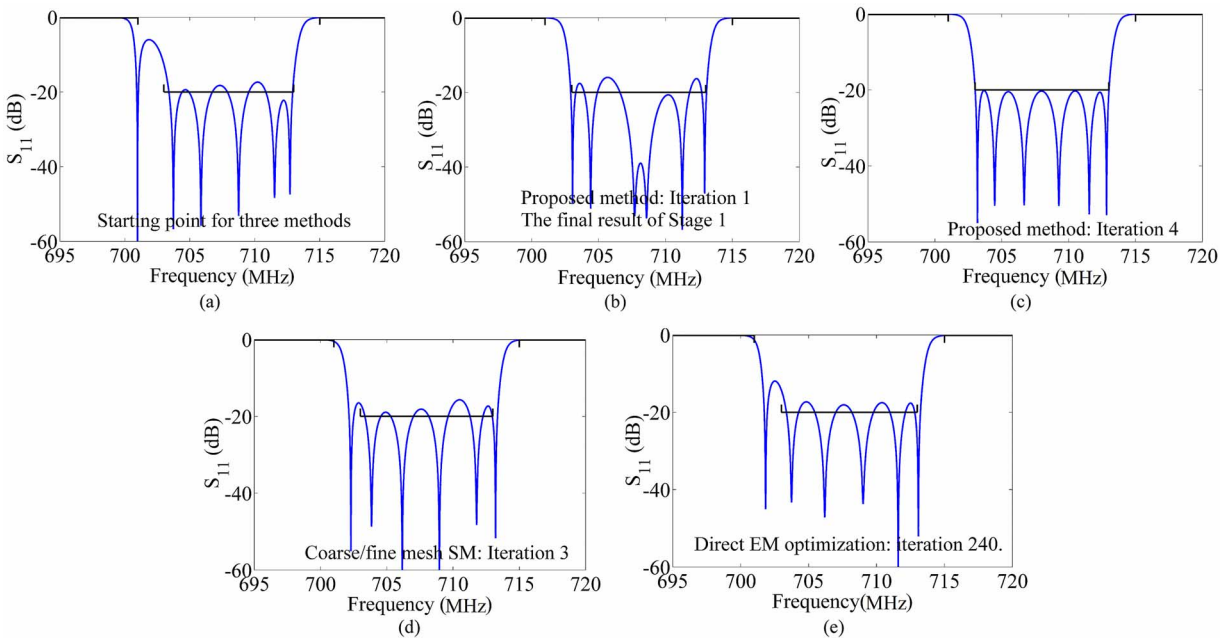

Fig. 11. Comparison of the results for three different optimization methods for the cavity filter example. (a) Starting point for all three methods. (b) Using our proposed space mapping method, all the feature frequencies move to the passband after the first stage. (c) Good equal-ripple response is obtained after four iterations, and our method can avoid being trapped in a local minimum. (d) Using coarse and fine mesh space mapping, the optimization process falls into a local minimum. (e) Using direct EM optimization, the optimization process falls into a local minimum.

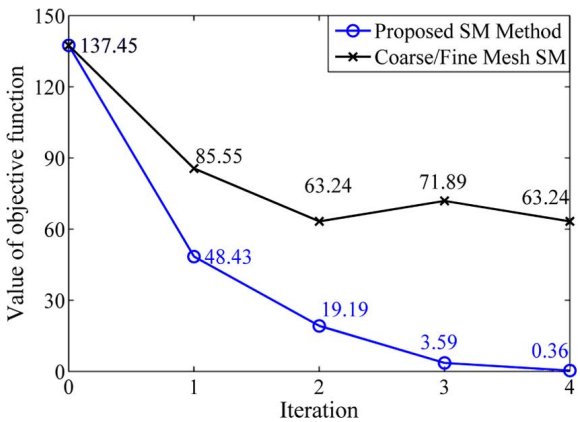

Fig. 12. Objective function values of the cavity filter response using: the proposed space mapping method (o) and coarse and fine mesh space mapping method (x). The objective function in the coarse and fine mesh space mapping optimization cannot be reduced further because it falls into a local minimum. Our proposed method can avoid being trapped in a local minimum and finds a good filter response in four iterations.

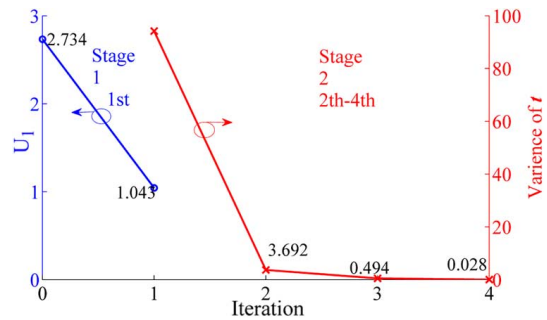

Fig. 13. Feature space objective functions U_1 and U_2 (i.e., $Var(\boldsymbol{t})$) for the cavity filter example. The first stage goes in the first iteration, and the second stage runs from the second iteration to the 4th iteration. Both U_1 and $Var(\boldsymbol{t})$ converges fast.

proposed method is shown in Fig. 7 and Table II, demonstrating that the proposed method has the shortest optimization time and best quality of solutions among the different methods compared.

B. Optimization of an Iris Coupled Microwave Cavity Filter

Consider an iris coupled cavity microwave bandpass filter shown in Fig. 10 [29]. The filter has seven geometrical design parameters described as follows. The heights of the big cylinders H_{c1}, H_{c2}, and H_{c3} positioned at the cavity centers are responsible for tuning the frequencies in the cavity. The required coupling bandwidths are accomplished via the iris widths W_1, W_2, W_3, and W_4 for a pre-tuning. The design variables are $\boldsymbol{x} = [W_1\ W_2\ W_3\ W_4\ H_{c1}\ H_{c2}\ H_{c3}]^T$.

EM evaluation is performed by the HFSS EM simulator using the fast simulation feature. We provide the design specifications $|S_{11}| < -20$ dB at a frequency range of 703–713 MHz and $|S_{21}| < -10$ dB at frequency range of 690–701 MHz and 715–720 MHz. The starting point is $\boldsymbol{x}^{(0)} = [115.289\ 51.276\ 46.897\ 51.084\ 42.816\ 50.287\ 50.402]^T$

TABLE III
COMPARISONS OF THREE METHODS FOR THE CAVITY FILTER

Optimization Method	Direct EM Optimization	Coarse/Fine Mesh Space Mapping	Proposed Space Mapping
No. of Iterations	240	3	4
Fine Model Evaluation Time	240 × 30min	4 × 30min	5 × 40min
Training Time	-	2 × 5h	4 × 1min
Design Optimization Time	-	3 × 4h	4 × 1min
Total Time	120 h	24 h	3 h 28min
Final Value of Objective Function	82.36 (being trapped in local minimum)	63.24 (being trapped in local minimum)	0.36

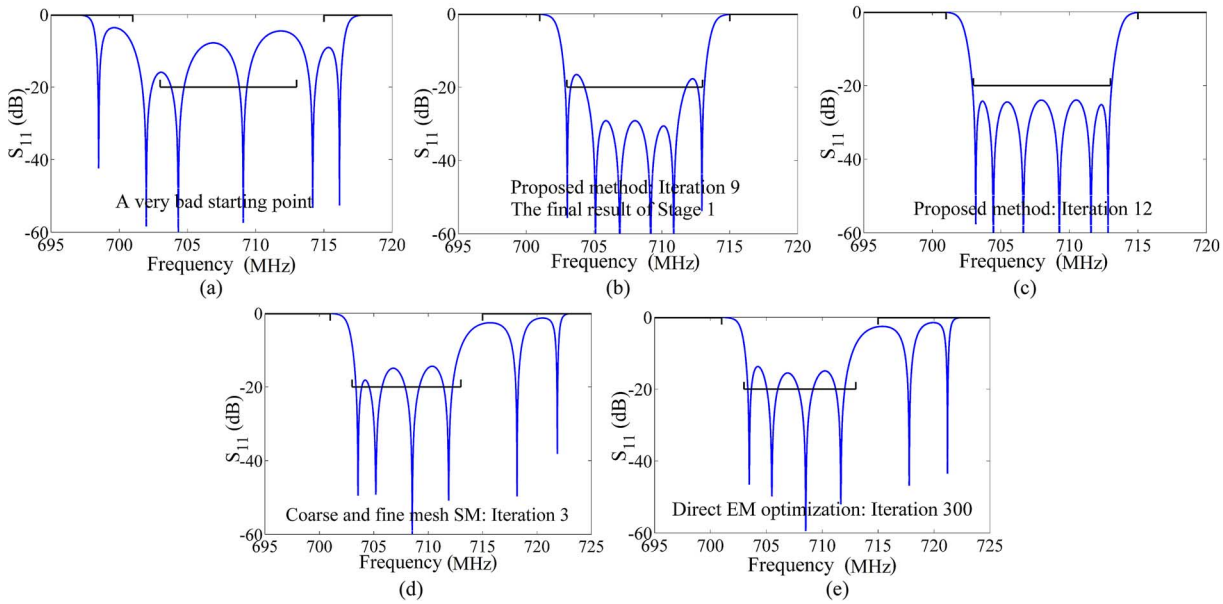

Fig. 14. Comparison of the results for three different optimization methods for the cavity filter example with bad starting point. (a) Very bad starting point for all three methods. (b) Using our proposed space mapping method, all the feature frequencies move to the passband after the first stage. (c) Good equal-ripple response is obtained after twelve iterations, and our method can avoid being trapped in a local minimum. (d) Using coarse and fine mesh space mapping, the optimization process falls into a local minimum. (e) Using direct EM optimization, the optimization process falls into a local minimum.

(all values in millimeters). From the second iteration, the $\boldsymbol{t}$ parameters are found to be $\boldsymbol{t}^{(2)} = [-16.787\ -14.932\ -32.553\ -22.344\ -17.701]^T$ (all values in decibels).

Using the proposed technique, the optimal solution $\boldsymbol{x}^{(4)} = [115.557\ 50.061\ 44.226\ 47.605\ 42.734\ 50.331\ 50.461]^T$ (all values in millimeters) is obtained after four iterations, and the final ripple vector $\boldsymbol{t}^{(4)} = [-20.16\ -20.48\ -20.32\ -20.28\ -20.60]^T$ (all values in decibels). The responses from the initial point, the first and the last iterations are shown in Fig. 11, from which we observe that our method can avoid being trapped in a local minimum and achieve a good equal-ripple filter response in four iterations. The values of objective function are shown in Fig. 12, which further shows our method avoids being trapped in a local minimum. We set the threshold $\varepsilon_2 = 0.3$. U_1 in the first stage and the variances of t in the second stage of our proposed method are shown in Fig. 13, and both U_1 and $Var(\boldsymbol{t})$ converge fast. From the final filter response in Fig. 11(c), we find that the best equal-ripple filter solution has already been found.

For comparison purposes, we use the coarse and fine mesh space mapping method [14] to optimize this filter, and the value of objective function for each iteration is shown in Fig. 12, from which we observe that the coarse and fine mesh space mapping optimization process falls into a local minimum. The comparison of the results for different methods, including direct EM optimization, coarse and fine mesh space mapping method and our proposed method is shown in Fig. 11 and Table III. Our proposed method uses 15 (i.e., $2N + 1$) EM simulations per iteration, which is more than by existing techniques, such as coarse and fine mesh space mapping. Because these 15 simulations are completely independent of each other, our technique is well suited for parallel computation, making the total computation time (40 min) for the 15 EM simulations to be only incrementally more than a single EM simulation (30 min). The total number of optimization iterations is much reduced in our technique because of the increased amount of useful information available from $2N + 1$ EM simulations in each iteration. Our space mapping method can increase the optimization efficiency and find a better result within less time compared with coarse and fine mesh EM space mapping and direct EM optimization.

As a further experiment on the robustness of the proposed optimization for this filter example, we use a much worse starting point $\boldsymbol{x}^{(0)} = [111.910\ 56.822\ 53.916\ 57.906\ 43.145\ 49.385\ 49.626]^T$ (all values in mm) to rerun our proposed method. Using the proposed technique, the optimal solution $\boldsymbol{x}^{(12)} = [119.331\ 51.953\ 45.099\ 48.278\ 41.881\ 50.186\ 50.385]^T$ (all values in mm) is obtained after 12 iterations, and the final ripple vector $\boldsymbol{t}^{(12)} = [-24.258\ -24.487\ -23.979\ -23.949\ -25.188]^T$ (all values in dB). The responses from initial point, the last iteration of the first stage and the last iterations are shown in Fig. 14(a)–(c), respectively. A preprocessing step was used to create a usable starting point, which is shown in Fig. 14(a), with correct number of feature frequencies. Fig. 14(b) shows that all of the feature frequencies move to the passband after the first stage. Fig. 14(c) shows that our proposed method can avoid being trapped in a local minimum and that a good equal-ripple filter response is obtained after 12 iterations. The values of objective function for all of the iterations are shown in Fig. 15. From the figure, we observe that using our proposed space mapping method the filter response can satisfy the design specifications in 11 iterations. U_1 in the first stage and the variances of $\boldsymbol{t}$ in the second stage of our proposed method are shown in Fig. 16. Both U_1 and $Var(\boldsymbol{t})$ converge fast.

For comparison purposes, we also use the baseline coarse and fine mesh space mapping optimization method [14] to optimize the filter, and the value of objective function for each iteration is shown in Fig. 15, from which we observe that the coarse and fine mesh space mapping optimization process falls

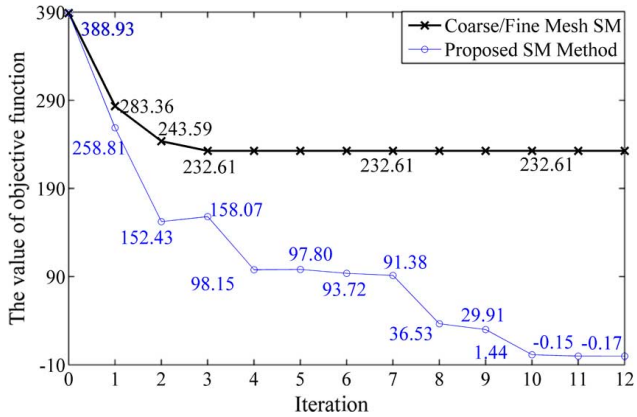

Fig. 15. Objective function values of the cavity filter response with bad starting point using: the proposed space mapping method (o) and coarse and fine mesh space mapping method (x). The objective function in the coarse and fine mesh space mapping optimization cannot be reduced further because it falls into a local minimum. Our proposed method can avoid being trapped in a local minimum and finds a good filter response in twelve iterations.

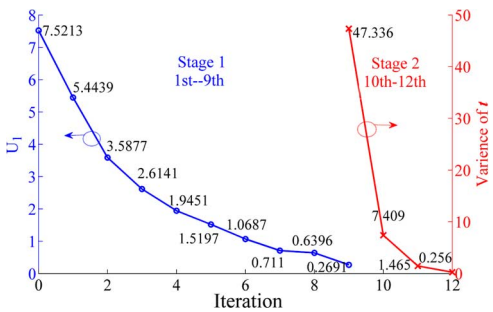

Fig. 16. Feature space objective functions U_1 and U_2 (i.e., $Var(\boldsymbol{t})$) for the cavity filter example with bad starting point. The first stage goes from the first iteration to the ninth iteration, and second stage runs from the tenth iteration to the twelfth iteration. Both U_1 and $Var(\boldsymbol{t})$ converge fast.

TABLE IV
COMPARISONS OF THREE METHODS FOR THE CAVITY FILTER WITH BAD STARTING POINT

Optimization Method	Direct EM Optimization	Coarse/Fine Mesh Space Mapping	Proposed Space Mapping
No. of Iterations	300	3	12
Fine Model Evaluation Time	300× 30min	4× 30min	(13+3*)× 40min
Training Time	-	2× 5h	12× 1min
Design Optimization Time	-	3× 4h	12× 1min
Total Time	150 h	24 h	11 h
Final Value of Objective Function	239.77 (being trapped in local minimum)	232.61 (being trapped in local minimum)	-0.17

*The number of EM simulations, which are not accepted during trust region adjustment.

into a local minimum. With the same starting point and same design specifications, the direct EM optimization is also performed for additional comparison. The direct EM optimization also falls into a local minimum with filter responses violating the design specifications. The comparison of the results for different methods, including direct EM optimization, coarse and fine mesh space mapping method and our proposed method is shown in Fig. 14 and Table IV. Our space mapping method can increase the optimization efficiency and find a better result within less time compared with coarse and fine mesh EM SM and direct EM optimization.

V. CONCLUSION

In this paper, a cognition-driven formulation of space mapping optimization of microwave filters has been proposed. In our method, two sets of intermediate feature space parameters, including the feature frequency and ripple height parameters, are used to build two kinds of mapping. A trust region approach has been incorporated to control the optimization updates, thus ensuring convergence of the proposed cognition-drive optimization. By using the proposed cognition-driven formulation of optimization directly in the feature space, our method can increase optimization efficiency and the ability to avoid being trapped in a local minimum over our baseline approaches of coarse and fine mesh EM space mapping and direct EM optimization. This technique is well-suited to the EM based design of Chebyshev- and elliptic-type filters, which are characterized by equal-ripple responses. We believe that further exploration of the cognition-driven formulation and the use of feature parameters for design optimization is highly promising. One possible future direction is to develop a systematic method for preprocessing the optimization starting point to correct the number of feature frequencies. Another possible direction is to incorporate more specific filter design knowledge into the cognition-driven formulation to further enhance optimization. The third possible direction is to expand the cognition-driven concept with more general feature parameters to advance EM based design beyond Chebyshev- and elliptic-type filters to more generic filters and other microwave circuits.

REFERENCES

[1] J.W. Bandler, R.M. Biernacki, S.H. Chen, P.A. Grobelny, and R. H. Hemmers, "Space mapping technique for electromagnetic optimization," *IEEE Trans. Microw. Theory Techn.*, vol. 42, no. 12, pp. 2536–2544, Dec. 1994.
[2] S. Koziel, Q. S. Cheng, and J. W. Bandler, "Space mapping," *IEEE Microw. Mag.*, vol. 9, no. 6, pp. 105–122, Dec. 2008.
[3] H. Kabir, L. Zhang, M. Yu, P. H. Aaen, J. Wood, and Q. J. Zhang, "Smart modeling of microwave devices," *IEEE Microw. Mag.*, vol. 11, no. 3, pp. 105–118, May 2010.
[4] J. W. Bandler, "Have you ever wondered about the engineer's mysterious 'feel' for a problem?," *IEEE Canadian Rev.*, no. 70, pp. 50–60, 2013, Summer.
[5] L. Zhang, P. H. Aaen, and J. Wood, "Portable space mapping for efficient statistical modeling of passive components," *IEEE Trans. Microw. Theory Techn.*, vol. 60, no. 3, pp. 441–450, Mar. 2012.
[6] R. B. Ayed, J. Gong, S. Brisset, F. Gillon, and P. Brochet, "Three-level output space mapping strategy for electromagnetic design optimization," *IEEE Trans. Magn.*, vol. 48, no. 2, pp. 671–674, Feb. 2012.
[7] S. Koziel, J. Meng, J. W. Bandler, M. H. Bakr, and Q. S. Cheng, "Accelerated microwave design optimization with tuning space mapping," *IEEE Trans. Microw. Theory Techn.*, vol. 57, no. 2, pp. 383–394, Feb. 2009.
[8] S. Koziel, "Shape-preserving response prediction for microwave design optimization," *IEEE Trans. Microw. Theory Techn.*, vol. 58, no. 11, pp. 2829–2837, Nov. 2010.
[9] F. Feng, C. Zhang, V. Gongal-Reddy, Q. J. Zhang, and J. Ma, "Parallel space-mapping approach to EM optimization," *IEEE Trans. Microw. Theory Techn.*, vol. 62, no. 5, pp. 1135–1148, May 2014.

[10] N. Leszczynska, L. Szydlowski, and M. Mrozowski, "Zero-pole space mapping for CAD of filters," *IEEE Microw. Wireless Comp. Lett.*, vol. 24, no. 9, pp. 581–583, Sep. 2014.
[11] J. Zhu, J. W. Bandler, N. K. Nikolova, and S. Koziel, "Antenna optimization through space mapping," *IEEE Trans. Antennas Propag.*, vol. 55, no. 3, pp. 651–658, Mar. 2007.
[12] J. W. Bandler, R. M. Biernacki, S. H. Chen, P. A. Grobelny, and R. H. Hemmers, "Exploitation of coarse grid for electromagnetic optimization," in *IEEE MTT-S Int. Microw. Symp. Dig.*, San Diego, CA, USA, May 1994, pp. 381–384.
[13] J. V. Morro, P. Soto, H. Esteban, V. E. Boria, C. Bachiller, M. Taroncher, S. Cogollos, and B. Gimeno, "Fast automated design of waveguide filters using aggressive space mapping with a new segmentation strategy and a hybrid optimization algorithm," *IEEE Trans. Microw. Theory Techn.*, vol. 53, no. 4, pp. 1130–1142, Apr. 2005.
[14] C. Zhang, F. Feng, and Q. J. Zhang, "EM optimization using coarse and fine mesh space mapping," in *Proc. Asia–Pacific Microw. Conf.*, Seoul, Korea, Nov. 2013, pp. 824–826.
[15] F. Feng, C. Zhang, V. Gongal-Reddy, and Q. J. Zhang, "Knowledge-based coarse and fine mesh space mapping approach to EM optimization," in *Proc. IEEE MTT-S Int. Conf. Numer. Electromagn. Modeling and Optimization*, Pavia, Italy, May 2014.
[16] S. Koziel and S. Ogurtsov, *Antenna Design by Simulation-Driven Optimization*. New York, NY, USA: Springer, 2014.
[17] M. H. Bakr, J. W. Bandler, N. Georgieva, and K. Madsen, "A hybrid aggressive space mapping algorithm for EM optimization," *IEEE Trans. Microw. Theory Techn.*, vol. 47, no. 12, pp. 2440–2449, Dec. 1999.
[18] S. Koziel, S. Ogurtsov, J. W. Bandler, and Q. S. Cheng, "Reliable space-mapping optimization integrated with EM-based adjoint sensitivities," *IEEE Trans. Microw. Theory Techn.*, vol. 61, no. 10, pp. 3493–3502, Oct. 2013.
[19] R. J. Cameron, C. M. Kudsia, and R. T. Mansour, *Microwave Filters for Communication Systems: Fundamentals, Design, Applications*. Hoboken, NJ, USA: Wiley, 2007.
[20] W. A. Atia, K. A. Zaki, and A. E. Atia, "Synthesis of general topology multiple coupled resonator filters by optimization," in *IEEE MTT-S Int. Microw. Symp. Dig.*, Jun. 1998, vol. 2, pp. 821–824.
[21] S. Amari, "Synthesis of cross-coupled resonator filters using an analytical gradient-based optimization technique," *IEEE Trans. Microw. Theory Techn.*, vol. 48, no. 9, pp. 1559–1564, Sep. 2000.
[22] P. Kozakowski and M. Mrozowski, "Automated CAD of coupled resonator filters," *IEEE Microw. Wireless Compon. Lett.*, vol. 12, no. 12, pp. 470–472, Dec. 2002.
[23] O. Glubokov and S. Koziel, "EM-driven tuning of substrate integrated waveguide filters exploiting feature-space surrogates," in *IEEE MTT-S Int. Microw. Symp. Dig.*, Tampa, FL, USA, Jun. 2014, pp. 1–3.
[24] S. Koziel and J. W. Bandler, "Feature-based statistical analysis for rapid yield estimation of microwave structures," in *IEEE MTT-S Int. Microw. Symp. Dig.*, Tampa, FL, USA, Jun. 2014, pp. 1–3.
[25] J. W. Bandler and S. H. Chen, "Circuit optimization: The state of the art," *IEEE Trans. Microw. Theory Techn.*, vol. 36, no. 2, pp. 424–443, Feb. 1988.
[26] N. M. Alexandrov, J. E. Dennis, R. M. Lewis, and V. Torczon, "A trust region framework for managing use of approximation models in optimization," *Struct. Multidisciplinary Optim.*, vol. 15, no. 1, pp. 16–23, 1998.
[27] M. H. Bakr, J. W. Bandler, R. M. Biernacki, S. H. Chen, and K. Madsen, "A trust region aggressive space mapping algorithm for EM optimization," *IEEE Trans. Microw. Theory Techn.*, vol. 46, no. 12, pp. 2412–2425, Dec. 1998.
[28] S. Koziel, J. W. Bandler, and Q. S. Cheng, "Robust trust-region space-mapping algorithms for microwave design optimization," *IEEE Trans. Microw. Theory Techn.*, vol. 58, no. 8, pp. 2166–2174, Aug. 2010.
[29] Y. Cao, S. Reitzinger, and Q. J. Zhang, "Simple and efficient high-dimensional parametric modeling for microwave cavity filters using modular neural network," *IEEE Microw. Wireless Compon. Lett.*, vol. 21, no. 5, pp. 258–260, May 2011.

Chao Zhang (S'14) was born on June 2, 1990, in Xinyang, Henan, China. He received the B.Eng. and M.Eng degrees from Tianjin University, Tianjin, China, in 2012 and 2014, respectively. He is currently working toward the Ph.D. degree in electronics at Carleton University, Ottawa, ON, Canada.

From February 2010 to June 2010, he was an exchange student with National Taipei University of Technology, Taipei, Taiwan. His research interests include electromagnetic simulation and optimization techniques, design and optimization of microwave circuits, space mapping, and surrogate model optimization.

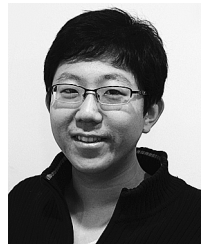

Feng Feng (S'13) was born on February 7, 1990, in Huludao, Liaoning, China. He received the B.Eng. degree from Tianjin University, Tianjin, China, in 2012. He is currently working the Ph.D. degree at Tianjin University, Tianjin, China.

He is also in a Ph.D. program of the Department of Electronics at Carleton University, Ottawa, ON, Canada. His research interests include microwave circuit design and modeling, optimization theory and algorithms, space mapping and surrogate model optimization, and electromagnetic field simulation and optimization.

Venu-Madhav-Reddy Gongal-Reddy was born on May 9, 1985, in Hyderabad, India. He received the B.Eng. degree from Jawaharlal Nehru Technological University, Hyderabad, India, in 2006, and the M.S. degree in radio frequency and microwave engineering from the Indian Institute of Technology, Kharagpur, India, in 2008. He is currently working toward the Ph.D. degree in electronics at Carleton University, Ottawa, ON, Canada.

His research interests include modeling, design, and optimization of microwave circuits, devices, and antennas.

Qi Jun Zhang (S'84–M'87–SM'95–F'06) received the B.Eng. degree from the Nanjing University of Science and Technology, Nanjing, China, in 1982, and the Ph.D. degree in electrical engineering from McMaster University, Hamilton, ON, Canada, in 1987.

From 1982 to 1983, he was with the System Engineering Institute, Tianjin University, Tianjin, China. From 1988 to 1990, he was with Optimization Systems Associates (OSA) Inc., Dundas, ON, Canada. In 1990, he joined the Department of Electronics, Carleton University, Ottawa, ON, Canada, where he is currently a Full Professor. On leave from Carleton University, he has also been with the School of Electronic Information Engineering, Tianjin University, Tianjin, China.

Dr. Zhang is a Fellow of the Electromagnetics Academy and the Canadian Academy of Engineering. He is a member of the Editorial Board of the IEEE TRANSACTIONS ON MICROWAVE THEORY AND TECHNIQUES. He is a member of the Technical Committee on CAD (MTT-1) of the IEEE Microwave Theory and Techniques Society (IEEE MTT-S).

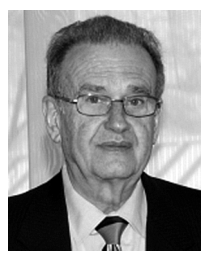

John W. Bandler (S'66–M'66–SM'74–F'78–LF'06) received the B.Sc.(Eng.), Ph.D., and D.Sc.(Eng.) degrees from the University of London, London, U.K., in 1963, 1967, and 1976, respectively.

He joined McMaster University, Hamilton, ON, Canada, in 1969. He is now a Professor Emeritus. He founded Optimization Systems Associates Inc. in 1983 and sold it to Hewlett-Packard in 1997. He is President of Bandler Corporation, Dundas, ON, Canada.

Dr. Bandler is a Fellow of several societies, including the Royal Society of Canada and the Canadian Academy of Engineering. He was the recipient of the IEEE Microwave Theory and Techniques (MTT-S) Microwave Application Award in 2004, the IEEE Canada McNaughton Gold Medal and the Queen Elizabeth II Diamond Jubilee Medal, both in 2012, the IEEE MTT-S Microwave Career Award in 2013, and McMaster University's Faculty of Engineering Research Achievement Award in 2014.